Rapid Communications

Imaging of nearly flat band induced atomic-scale negative differential conductivity in *ABC*-stacked trilayer graphene

Long-Jing Yin,[1,*] Li-Zhen Yang,[1] Li Zhang,[1] Qilong Wu,[1] Xiaoshuai Fu,[1] Ling-Hui Tong,[1] Guang Yang,[2,†] Yuan Tian,[1] Lijie Zhang,[1] and Zhihui Qin[1,‡]

[1]*Key Laboratory for Micro/Nano Optoelectronic Devices of Ministry of Education and Hunan Provincial Key Laboratory of Low-Dimensional Structural Physics and Devices, School of Physics and Electronics, Hunan University, Changsha 410082, China*

[2]*School of Sciences, Hebei University of Science and Technology, Shijiazhuang 050018, China*

(Received 1 October 2020; revised 17 November 2020; accepted 23 November 2020; published 8 December 2020)

Despite recent transport studies of *ABC*-stacked multilayer graphene systems revealed various unusual quantum phenomena which arise from the nearly flat electronic bands, their quantum tunneling properties have rarely been addressed. Here we investigate the local tunneling characteristics of a gapped *ABC*-stacked trilayer graphene (TLG) and report the experimental observation of the nearly flat band induced atomic-site-dependent negative differential conductivity (NDC, characterized by a current drop with increasing voltage) via scanning tunneling spectroscopy (STS) measurements. We show that strong NDC emerges in the gap region next to a sharp STS peak induced by the very flat low-energy dispersion of *ABC* TLG. The NDC is found to mainly reside on one atomic sublattice of the surface layer due to the strong sublattice and layer localization of the nearly flat bands. The observed NDC behavior is explained by the tunnel-diode mechanism, namely, the coexistence of a sharp flat-dispersion STS peak in which tunneling is strongly enhanced and a subsequent gap region in which tunneling is forbidden. Furthermore, we also find that a local defect could effectively switch off the NDC over a large spatial range. Our result highlights a quantum tunneling effect unique to the graphene-based nearly flat band system and expands the potential application scope of *ABC* TLG.

DOI: 10.1103/PhysRevB.102.241403

Recently, multilayer graphene systems with nearly flat low-energy bands have attracted considerable attention due to the flat band induced exotic electronic properties [1–5]. *ABC* (or rhombohedral)-stacked trilayer graphene (TLG) is predicted to be one such particular material, as it possesses an unusual dispersion of $E \sim k^3$ (k is the wave vector) with nearly nondispersive flat bands around the charge neutrality point (CNP) which has a local extension near the K point of the Brillouin zone [6]. Such nearly flat bands host diverging density of states (DOS) and are supposed to afford strong electron-electron interactions; thus they can lead to various novel quantum phenomena [7–12]. Very recently, transport experiments reported flat band induced correlated insulator states and signatures of superconductivity in *ABC*-stacked TLG aligned to *h*-BN [13,14], as well as intrinsic magnetism in both *ABC* TLG/*h*-BN heterostructure [15] and suspended *ABC* TLG [16]. These great successes demonstrate the remarkable quantum transport properties of flat bands in the *ABC*-stacked graphene system. However, the quantum tunneling properties of graphene-based nearly flat band materials have, so far, rarely been addressed.

In this work, we focus on the quantum tunneling characteristics of *ABC*-stacked TLG and demonstrate a unique tunneling phenomenon: nearly flat band induced atomic-site-dependent negative differential conductance (NDC). NDC, characterized by decreasing current with increasing voltage, is one of the most fascinating tunneling phenomena which can enable a wide range of potential applications [17,18]. Though it has been seen in a variety of systems [19–25], the tunneling-based NDC is not common in graphene [26–28]. We report an observation of NDC in *ABC*-stacked TLG using scanning tunneling microscopy (STM) and spectroscopy (STS) measurements. The studied *ABC* TLG shows a small gap, generated by the substrate- and tip-induced interlayer potential, and almost flat dispersions at the two edges of the band gap with the DOS of these two locally flat bands (or two van Hove singularities) respectively localized on the opposite sublattices of the outermost layers. Strong NDC is observed, from the STS spectra, in the gap region next to a sharp DOS peak formed by the very flat dispersion. The observed NDC shows an atomic site dependence, that is, NDC on one sublattice and non-NDC on the other sites of the top layer, owing to the sublattice localization of the nearly flat bands. The tunneling spectroscopy combined with theoretical simulation indicates that the observed NDC effect originates from the tunnel-diode mechanism.

The TLG sample used in our experiment is an electronically decoupled graphene flake on a highly oriented pyrolytic graphite (HOPG) substrate prepared by surface exfoliation. The STM and STS measurements were carried out at 77 K using a commercial ultrahigh-vacuum STM from CreaTec (see the Supplemental Material [29] for details of sample

*yinlj@hnu.edu.cn
†gyangphys@hebust.edu.cn
‡zhqin@hnu.edu.cn

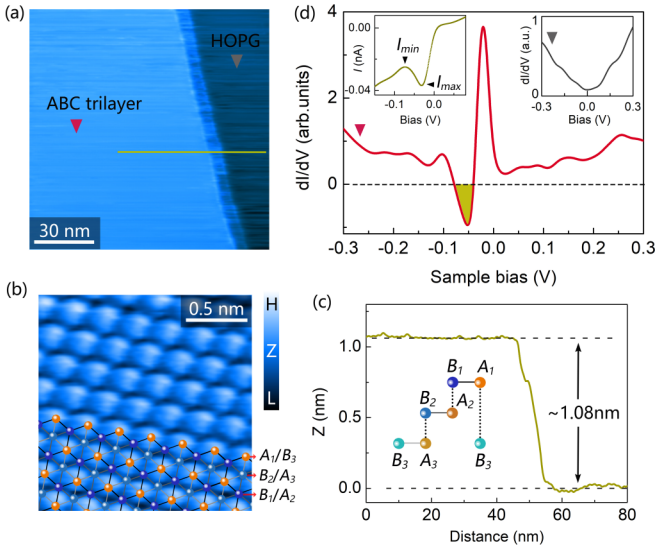

FIG. 1. (a) A STM topographic image ($120 \times 120\,\mathrm{nm}^2$, $V_b = 0.4\,\mathrm{V}$, $I = 0.1\,\mathrm{nA}$) of *ABC*-stacked TLG on graphite, which shows a step edge in the right region of the image. (b) Atomic-resolution image ($V_b = 0.2\,\mathrm{V}$, $I = 0.1\,\mathrm{nA}$) of the *ABC* TLG shown in (a). The *ABC*-stacking configuration is superimposed with part of the image. Colored balls denote carbon atoms. Black, gray, and light gray lines indicate C-C bonds in the top, middle, and bottom layer, respectively. (c) A representative height profile across the step along the straight line in (a), showing the height difference of the step ~1.08 nm. We measured more than 20 line cuts at different regions along the step edge. Those regions with obvious scanning-induced fluctuations are avoided. Inset shows the side view of the *ABC*-stacking configuration. (d) A typical *dI/dV* spectrum and the corresponding *I-V* spectrum (left inset) of *ABC* TLG obtained on the A_1 site from (a). Dashed line denotes the position of zero conductance. The yellow region highlights NDC. Right inset is the *dI/dV* spectrum recorded at the graphite bulk region in (a).

preparation and measurements). Figures 1(a) and 1(b), respectively, show representative large area and atomic-resolution STM topographic images of the decoupled *ABC*-stacked TLG flake on graphite. For the *ABC*-stacked TLG, the adjacent layers are both *AB* stacked; i.e., the B_1 and B_2 sublattices of the upper layers are, respectively, right above the A_2 and A_3 sublattices of the underlying layers, and the upper-layer *A* sublattices lie at the center of the lower-layer hexagons. Therefore, we obtained a triangular lattice in the atomic-resolution image [Fig. 1(b)] of the *ABC* TLG surface due to the asymmetry of *A*/*B* sublattices, consistent with that reported previously [30–33]. The large area image Fig. 1(a) visualizes a step edge of the *ABC* TLG flake. The step height is measured about 1.08 ± 0.04 nm [Fig. 1(c)], which is slightly larger than the normal value of three graphene layers (~1.02 nm). As demonstrated in previous works [31,34–37], such an increased interlayer spacing could efficiently decouple the *ABC* TLG flake from the underlying graphite bulk, leading to the result that the top flake behaves as freestanding *ABC* TLG (identified by the STS spectra below).

Figure 1(d) shows representative STS (dI/dV–V) spectra measured on the *ABC* TLG region (on the A_1 site) and the graphite substrate region in Fig. 1(a). The STS spectrum provides direct access to the local DOS of electrons beneath the STM tip. The STS curve obtained from the substrate region [right inset of Fig. 1(d)] shows a typical spectrum of Bernal graphite, i.e., a V-shaped structure with finite tunneling conductance near the Fermi energy [34]. The STS spectrum recorded on the *ABC* TLG region displays a sharp and pronounced DOS peak located near the Fermi energy. The sharp DOS peak is attributed to the nearly flat band structure near the CNP of the *ABC* TLG, as reported previously in Refs. [30–32]. Such a nearly flat band induced peak in the STS spectrum can be seen as a fingerprint of *ABC*-stacked multilayer graphene [38], indicating that the graphene flake shown in Fig. 1(a) is a decoupled *ABC*-stacked TLG. Below we will show that this DOS peak plays an important role in the emergence of NDC. Further support for the *ABC* configuration can be obtained from Fig. S2 in which an *ABA*-*ABC* stacking domain wall is discovered near the studied *ABC* TLG region (see Supplemental Material [29] for more details). The above results demonstrate explicitly that the top multilayer flake in Fig. 1(a) is a decoupled *ABC*-stacked TLG.

A more remarkable feature revealed in the STS spectrum of the *ABC* TLG region is the existence of NDC. The differential conductance shown in Fig. 1(d) exhibits negative values at the bias voltage around −50 mV next to the sharp DOS peak, indicating strong NDC. The NDC characteristic also can be reflected directly in the *I-V* spectrum [left inset of Fig. 1(d)] as decreasing current with increasing bias voltage. In our experiment, we find a close correlation between the NDC and the sharp flat dispersion induced DOS peak, i.e., the emergence of NDC always accompanies the sharp and strong DOS peak. This is obtained by measuring atomic-scale spectroscopy in the *ABC* TLG. Figures 2(a) and 2(b) show the *dI/dV* and the corresponding *I-V* spectra taken at three different atomic sites of the *ABC* unit cell. In *ABC* TLG, the surface electronic states of nearly flat bands are localized at one sublattice of the top layer [38]. Therefore, we observed a sharp and pronounced DOS peak (at ~−20 mV) on the A_1 site and a much weaker DOS peak on the B_1 and B_2 sites [Fig. 2(a)]. Interestingly, the NDC also mainly exists in the spectrum (around −50 mV) of the A_1 site and almost vanishes in the spectra of other sites [see Figs. 2(a) and 2(b), and the contour plot in the inset of Fig. 2(a)]. To clearly show the relationship between the NDC and the atomic sites, we directly imaged the NDC in real space by operating atomic-scale STS mapping. Figure 2(c) shows the atomic-scale STS map recorded at −50 mV as well as the simultaneously measured topographic image. Obviously, strong negative conductance (dark blue color) is visualized predominantly on the A_1 site and is nearly surrounded by positive conductance of other sites. Besides, the NDC is not observed in the STS map taken at other voltages [see Fig. 2(d) for 220 mV map]. The spatial variation of the spectra rules out the effect of the STM tip as the origin of NDC, and the above measurements strongly suggest that the observed NDC is closely related to the localized flat-dispersion states on the A_1 site.

To explore the origin of the NDC, we further examine the STS spectra of the *ABC* TLG in Fig. 2(a). A small shoulder peak can be observed at ~−0.1 V in the left side of the NDC region for all STS spectra. Furthermore, the tunneling conductance between the shoulder peak and the sharp flat-dispersion

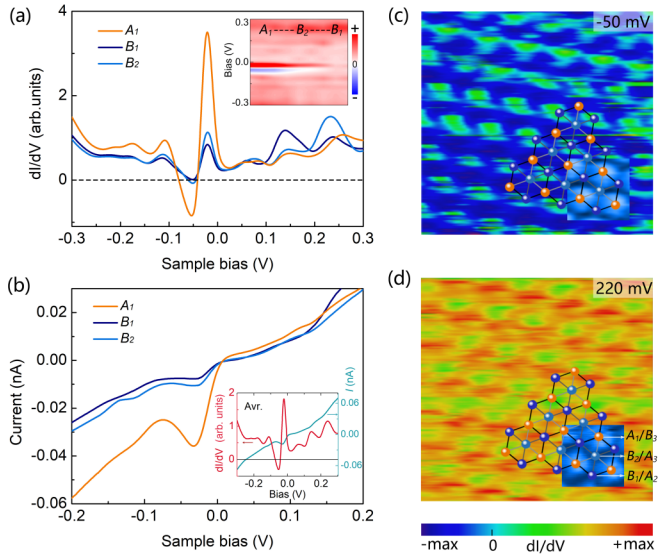

FIG. 2. Atomic-site-dependent *dI*/*dV* spectra (a) and corresponding *I*-*V* spectra (b) of *ABC* TLG. Inset in (a) shows the contour plot of *dI*/*dV* spectra along the A_1-B_2-B_1 direction. Inset in (b) shows the spatial average *dI*/*dV* and *I*-*V* spectra for (a) and (b). NDC still can be clearly observed in the average spectrum, suggesting the robustness of NDC in *ABC* TLG. (c), (d) *dI*/*dV* spatial maps ($1.5 \times 1.5\,\mathrm{nm}^2$) measured at the energies of −50 meV (c) and 220 meV (d). The insets are simultaneously obtained topographic images superimposed with the atomic structure of *ABC* TLG.

peak is low and it vanishes at −50 mV for the spectrum absent of NDC. These typical spectroscopic characteristics indicate that the *ABC* TLG is gapped at −50 mV [33]. In our *ABC* TLG, the underlying graphite substrate [31] together with the STM tip [39,40] introduce an interlayer potential which breaks the inversion symmetry of *ABC* TLG; then a small energy gap is opened at the CNP (at ∼−50 mV) [41–44]. Meanwhile, the highly flat band structures near the CNP split into two dispersionless parts at the conduction- and valance-band edges flanking the energy gap [see Fig. 3(a)]. The electronic states from these two almost dispersionless bands are theorized to be localized only on the opposite sublattices of the outermost layers [Fig. 3(a)] [45]. Consequently, we only

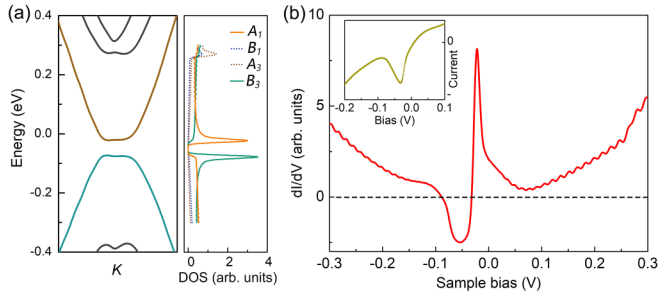

FIG. 3. (a) Theoretical band structure (left panel) and site-resolved DOS (right panel) of the gapped *ABC*-stacked TLG under a 0.06 V interlayer potential (Supplemental Material [29]). Only the DOS of those atomic sites in the outermost layers are presented. (b) Simulated *dI*/*dV* spectrum and *I*-*V* curve (inset) via the proposed model.

measured one sharp DOS peak generated by the nearly flat conduction-band edge in the top layer, that is, the peak at ∼−20 mV localized on the A_1 site, as the STS predominantly probes the DOS of the surface. The small shoulder peak at ∼−0.1 V thus can be attributed to the very flat valance-band edge residing on the B_3 site of the bottom layer. That is why the intensity of this state measured on the A_1 site is slightly stronger than that on the B_1 and B_2 sites, because the B_3 site is right under the A_1 site [see inset of Fig. 1(c)]. Such a layer-polarization phenomenon has already been seen in *ABC*-stacked TLG [31,33] and is similar to that observed in Bernal bilayer graphene [27,35–37,46–48].

According to the analysis of the tunneling spectroscopy, the observed NDC in our experiment now can be qualitatively explained by the tunnel-diode mechanism. In such a mechanism, NDC has been shown to arise from the existence of an energy level at which tunneling is effectively favored and a followed level at which tunneling is forbidden (or suppressed) [19]. In our experiment, when the sample bias matches the sharp nearly flat band peak near −20 mV, the tunneling probability is strongly enhanced and the tunneling current reaches a local maximum [marked by $I_{\max}$ in the inset of Fig. 1(d)]. Upon the increase in the bias, the nearly flat band state moves away, the tunneling probability is significantly reduced at the gap region, and the tunneling current effectively decreases (reaching $I_{\min}$), thus leading to the NDC. Namely, the sharp nearly flat band state and the small energy gap provide the two key conditions for the emergence of the NDC. It is worth stressing that to generate NDC, the nearly flat band induced DOS peak should be sufficiently sharp and strong. As shown in Fig. 2(a), no clear NDC is observed on the B_1 and B_2 sites, even though the flat-dispersion DOS peak still exists (due to the finite spatial extent of the wave function) but with a much weaker intensity (∼4 times smaller). A similar result has also been observed for Landau level induced NDC in monolayer graphene for which NDC is only detected accompanying those Landau levels with large height-to-width ratio [49].

To quantitatively verify the above mechanism for the sharp flat-dispersion DOS peak induced atomic-scale NDC, we carried out theoretical simulations by using the standard *I*-*V* formula: $I(V,z) \propto \int_{E_F-V}^{E_F} \rho_S(E+V)\rho_T(E)T(E,V,z)dE$. Here $T(E,V,z)$ is the tunneling matrix element, $z \approx 1$ nm is the tunnel barrier width (i.e., tip-sample distance), and ρ_S and ρ_T are the sample and tip DOS, respectively. Using the Wentzel-Kramers-Brillouin approximation, the tunneling matrix element can be estimated as $T(E,V,z) = \exp[-2\sqrt{2(\Phi - V/2 - E)}z]$, where Φ is the work function. The sample DOS is obtained from A_1 site by calculation [Fig. 3(a)] and the tip DOS is modeled to have a localized state near E_F; these are both based on previous theoretical models [20,27,45]. The simulated *I*-*V* curve and the corresponding *dI*/*dV* curve are shown in Fig. 3(b). The plots nicely reproduce the observed NDC behavior, confirming the validity of the proposed mechanism.

Motivated by a recent work in bilayer graphene [27], we further investigated the influence of defects on tuning NDC. Figure 4 shows the STS spectra measured near a local defect in the *ABC* TLG at A_1 sites of different positions. Obviously, NDC completely disappears in the gap region for the spectra taken at 15 and 12 nm away from the defect. Moreover, the

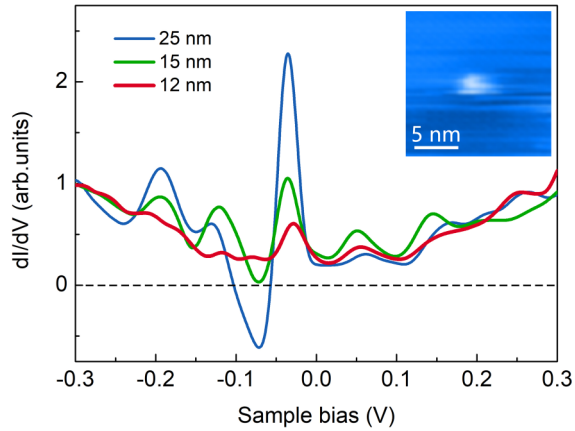

FIG. 4. *dI/dV* spectra of A_1 site taken at three different regions about 25, 15, and 12 nm away from a defect shown in the inset. The defect could be either an adsorption or a lattice defect. Dashed straight line indicates the position of zero conductance.

intensity of the flat-dispersion DOS peak at ~ -20 mV is dramatically suppressed near the defect. Such observations indicate a clear association between the sharp STS peak and the NDC, further supporting our proposed mechanism of NDC. The strong impact of a defect in the low-energy electronic properties of *ABC* TLG can be attributed to the scattering and interference of charge carriers near defects, analogous to that found in bilayer graphene [27]. It is worth noting that, under the influence of defects, the NDC behavior observed in bilayer graphene only entirely vanishes at the region right next to the defect, while it is extinguished at the locations more than 10 nm away from the defect in our experiment. This result may suggest that the quasiparticle scattering and interference has a greater influence on the *ABC*-stacked TLG [50]. Consequently, a local defect can be used to switch off the NDC over a large range in *ABC* TLG.

In summary, we reported the nearly flat band induced atomic-scale NDC in *ABC*-stacked TLG. The locally almost-dispersionless and layer-polarized flat low-energy bands of a gapped *ABC* TLG result in a sharp DOS peak at the gap edge in the STS spectra localizing on one sublattice of the surface layer. The greatly enhanced tunneling at the sharp flat-dispersion peak followed by the suppressed tunneling at the nearby gap region generates a strong NDC residing only on the surface A_1 site. Our experiment demonstrated that a local defect can be used to switch off the NDC over a large spatial range in *ABC* TLG. Our result provides timely understanding of quantum tunneling of nearly flat bands in *ABC*-stacked graphene and suggests the potential application of *ABC*-stacked graphene tunneling devices.

This work was supported by the National Natural Science Foundation of China (Grants No. 11804089, No. 11904094, No. 51772087, and No. 51972106), the Natural Science Foundation of Hunan Province, China (Grants No. 2018JJ3025, No. 2019JJ50034, and No. 2019JJ50073), and the Strategic Priority Research Program of Chinese Academy of Sciences (Grant No. XDB30000000). The authors acknowledge the financial support from the Fundamental Research Funds for the Central Universities of China.

[1] Y. Cao, V. Fatemi, S. Fang, K. Watanabe, T. Taniguchi, E. Kaxiras, and P. Jarillo-Herrero, Unconventional superconductivity in magic-angle graphene superlattices, Nature **556**, 43 (2018).

[2] Y. Cao, V. Fatemi, A. Demir, S. Fang, S. L. Tomarken, J. Y. Luo, J. D. Sanchez-Yamagishi, K. Watanabe, T. Taniguchi, E. Kaxiras, R. C. Ashoori, and P. Jarillo-Herrero, Correlated insulator behaviour at half-filling in magic-angle graphene superlattices, Nature **556**, 80 (2018).

[3] M. Serlin, C. L. Tschirhart, H. Polshyn, Y. Zhang, J. Zhu, K. Watanabe, T. Taniguchi, L. Balents, and A. F. Young, Intrinsic quantized anomalous Hall effect in a moiré heterostructure, Science **367**, 900 (2020).

[4] X. Liu, Z. Hao, E. Khalaf, J. Y. Lee, Y. Ronen, H. Yoo, D. Haei Najafabadi, K. Watanabe, T. Taniguchi, A. Vishwanath, and P. Kim, Tunable spin-polarized correlated states in twisted double bilayer graphene, Nature **583**, 221 (2020).

[5] C. Shen, Y. Chu, Q. Wu, N. Li, S. Wang, Y. Zhao, J. Tang, J. Liu, J. Tian, K. Watanabe, T. Taniguchi, R. Yang, Z. Y. Meng, D. Shi, O. V. Yazyev, and G. Zhang, Correlated states in twisted double bilayer graphene, Nat. Phys. **16**, 520 (2020).

[6] F. Zhang, B. Sahu, H. Min, and A. H. MacDonald, Band structure of *ABC*-stacked graphene trilayers, Phys. Rev. B **82**, 035409 (2010).

[7] R. Olsen, R. van Gelderen, and C. M. Smith, Ferromagnetism in *ABC*-stacked trilayer graphene, Phys. Rev. B **87**, 115414 (2013).

[8] N. B. Kopnin, M. Ijäs, A. Harju, and T. T. Heikkilä, High-temperature surface superconductivity in rhombohedral graphite, Phys. Rev. B **87**, 140503(R) (2013).

[9] H. Wang, J.-H. Gao, and F.-C. Zhang, Flat band electrons and interactions in rhombohedral trilayer graphene, Phys. Rev. B **87**, 155116 (2013).

[10] B. L. Chittari, G. Chen, Y. Zhang, F. Wang, and J. Jung, Gate-Tunable Topological Flat Bands in Trilayer Graphene Boron-Nitride Moiré Superlattices, Phys. Rev. Lett. **122**, 016401 (2019).

[11] Y.-H. Zhang and T. Senthil, Bridging Hubbard model physics and quantum Hall physics in trilayer graphene/*h*-BN moiré superlattice, Phys. Rev. B **99**, 205150 (2019).

[12] Y. Lee, D. Tran, K. Myhro, J. Velasco, N. Gillgren, C. N. Lau, Y. Barlas, J. M. Poumirol, D. Smirnov, and F. Guinea, Competition between spontaneous symmetry breaking and single-particle gaps in trilayer graphene, Nat. Commun. **5**, 5656 (2014).

[13] G. Chen, L. Jiang, S. Wu, B. Lyu, H. Li, B. L. Chittari, K. Watanabe, T. Taniguchi, Z. Shi, J. Jung, Y. Zhang, and F. Wang, Evidence of a gate-tunable Mott insulator in a trilayer graphene moiré superlattice, Nat. Phys. **15**, 237 (2019).

[14] G. Chen, A. L. Sharpe, P. Gallagher, I. T. Rosen, E. J. Fox, L. Jiang, B. Lyu, H. Li, K. Watanabe, T. Taniguchi, J. Jung, Z. Shi, D. Goldhaber-Gordon, Y. Zhang, and F. Wang, Signatures of tunable superconductivity in a trilayer graphene moiré superlattice, Nature **572**, 215 (2019).

[15] G. Chen, A. L. Sharpe, E. J. Fox, Y. H. Zhang, S. Wang, L. Jiang, B. Lyu, H. Li, K. Watanabe, T. Taniguchi, Z. Shi, T. Senthil, D. Goldhaber-Gordon, Y. Zhang, and F. Wang, Tunable correlated Chern insulator and ferromagnetism in a moiré superlattice, Nature **579**, 56 (2020).

[16] Y. Lee, S. Che, J. J. Velasco, D. Tran, J. Baima, F. Mauri, M. Calandra, M. Bockrath, and C. N. Lau, Gate tunable magnetism and giant magnetoresistance in *ABC*-stacked few-layer graphene, arXiv:1911.04450.

[17] L. Esaki, New phenomenon in narrow germanium $p-n$ junctions, Phys. Rev. **109**, 603 (1958).

[18] L. L. Chang, L. Esaki, and R. Tsu, Resonant tunneling in semiconductor double barriers, Appl. Phys. Lett. **24**, 593 (1974).

[19] P. Bedrossian, D. M. Chen, K. Mortensen, and J. A. Golovchenko, Demonstration of the tunnel-diode effect on an atomic scale, Nature (London, UK) **342**, 258 (1989).

[20] I. W. Lyo and P. Avouris, Negative differential resistance on the atomic scale: Implications for atomic scale devices, Science **245**, 1369 (1989).

[21] B. W. Heinrich, M. V. Rastei, D. J. Choi, T. Frederiksen, and L. Limot, Engineering Negative Differential Conductance with the Cu(111) Surface State, Phys. Rev. Lett. **107**, 246801 (2011).

[22] X. W. Tu, G. Mikaelian, and W. Ho, Controlling Single-Molecule Negative Differential Resistance in a Double-Barrier Tunnel Junction, Phys. Rev. Lett. **100**, 126807 (2008).

[23] M. Rashidi, M. Taucer, I. Ozfidan, E. Lloyd, M. Koleini, H. Labidi, J. L. Pitters, J. Maciejko, and R. A. Wolkow, Time-Resolved Imaging of Negative Differential Resistance on the Atomic Scale, Phys. Rev. Lett. **117**, 276805 (2016).

[24] Y. C. Lin, R. K. Ghosh, R. Addou, N. Lu, S. M. Eichfeld, H. Zhu, M. Y. Li, X. Peng, M. J. Kim, L. J. Li, R. M. Wallace, S. Datta, and J. A. Robinson, Atomically thin resonant tunnel diodes built from synthetic van der Waals heterostructures, Nat. Commun. **6**, 7311 (2015).

[25] M. L. Perrin, R. Frisenda, M. Koole, J. S. Seldenthuis, J. A. Gil, H. Valkenier, J. C. Hummelen, N. Renaud, F. C. Grozema, J. M. Thijssen, D. Dulic, and H. S. van der Zant, Large negative differential conductance in single-molecule break junctions, Nat. Nanotechnol. **9**, 830 (2014).

[26] L. Britnell, R. V. Gorbachev, A. K. Geim, L. A. Ponomarenko, A. Mishchenko, M. T. Greenaway, T. M. Fromhold, K. S. Novoselov, and L. Eaves, Resonant tunnelling and negative differential conductance in graphene transistors, Nat. Commun. **4**, 1794 (2013).

[27] K. S. Kim, T. H. Kim, A. L. Walter, T. Seyller, H. W. Yeom, E. Rotenberg, and A. Bostwick, Visualizing Atomic-Scale Negative Differential Resistance in Bilayer Graphene, Phys. Rev. Lett. **110**, 036804 (2013).

[28] Y. Wu, D. B. Farmer, W. Zhu, S.-J. Han, C. D. Dimitrakopoulos, A. A. Bol, P. Avouris, and Y.-M. Lin, Three-terminal graphene negative differential resistance devices, ACS Nano **6**, 2610 (2012).

[29] See Supplemental Material at http://link.aps.org/supplemental/10.1103/PhysRevB.102.241403 for more experimental data showing an *ABA*-*ABC* stacking domain wall and position-dependent STS spectra, details of band structure and local DOS calculations, and analysis.

[30] R. Xu, L.-J. Yin, J.-B. Qiao, K.-K. Bai, J.-C. Nie, and L. He, Direct probing of the stacking order and electronic spectrum of rhombohedral trilayer graphene with scanning tunneling microscopy, Phys. Rev. B **91**, 035410 (2015).

[31] L.-J. Yin, W.-X. Wang, Y. Zhang, Y.-Y. Ou, H.-T. Zhang, C.-Y. Shen, and L. He, Observation of chirality transition of quasiparticles at stacking solitons in trilayer graphene, Phys. Rev. B **95**, 081402(R) (2017).

[32] L.-J. Yin, L.-J. Shi, S.-Y. Li, Y. Zhang, Z.-H. Guo, and L. He, High-Magnetic-Field Tunneling Spectra of *ABC*-Stacked Trilayer Graphene on Graphite, Phys. Rev. Lett. **122**, 146802 (2019).

[33] M. Yankowitz, F. Wang, C. N. Lau, and B. J. LeRoy, Local spectroscopy of the electrically tunable band gap in trilayer graphene, Phys. Rev. B **87**, 165102 (2013).

[34] G. Li, A. Luican, and E. Y. Andrei, Scanning Tunneling Spectroscopy of Graphene on Graphite, Phys. Rev. Lett. **102**, 176804 (2009).

[35] L.-J. Yin, S.-Y. Li, J.-B. Qiao, J.-C. Nie, and L. He, Landau quantization in graphene monolayer, Bernal bilayer, and Bernal trilayer on graphite surface, Phys. Rev. B **91**, 115405 (2015).

[36] L.-J. Yin, Y. Zhang, J.-B. Qiao, S.-Y. Li, and L. He, Experimental observation of surface states and Landau levels bending in bilayer graphene, Phys. Rev. B **93**, 125422 (2016).

[37] L.-J. Yin, L.-J. Shi, L.-Z. Yang, L.-H. Tong, and L. He, Spectroscopic characterization of Landau-level splitting and the intermediate $\upsilon = 0$ phase in bilayer graphene, Phys. Rev. B **101**, 165418 (2020).

[38] D. Pierucci, H. Sediri, M. Hajlaoui, J.-C. Girard, T. Brumme, M. Calandra, E. Velez-Fort, G. Patriarche, M. G. Sill, G. Ferro, V. Soulière, M. Marangolo, F. Sirotti, F. Mauri, and A. Ouerghi, Evidence for flat bands near the Fermi level in epitaxial rhombohedral multilayer graphene, ACS Nano **9**, 5432 (2015).

[39] F. Ghahari, D. Walkup, C. Gutiérrez, J F. Rodriguez-Nieva, Y. Zhao, J. Wyrick, F D. Natterer, W G. Cullen, K. Watanabe, T. Taniguchi, L. S. Levitov, N. B. Zhitenev, and J. A. Stroscio, An on/off Berry phase switch in circular graphene resonators, Science **356**, 845 (2017).

[40] Y. Jiang, J. Mao, D. Moldovan, M. R. Masir, G. Li, K. Watanabe, T. Taniguchi, F. M. Peeters, and E. Y. Andrei, Tuning a circular $p-n$ junction in graphene from quantum confinement to optical guiding, Nat. Nanotechnol. **12**, 1045 (2017).

[41] C. H. Lui, Z. Li, K. F. Mak, E. Cappelluti, and T. F. Heinz, Observation of an electrically tunable band gap in trilayer graphene, Nat. Phys. **7**, 944 (2011).

[42] W. Bao, L. Jing, J. Velasco, Y. Lee, G. Liu, D. Tran, B. Standley, M. Aykol, S. B. Cronin, D. Smirnov, M. Koshino, E. McCann, M. Bockrath, and C. N. Lau, Stacking-dependent band gap and quantum transport in trilayer graphene, Nat. Phys. **7**, 948 (2011).

[43] K. Zou, F. Zhang, C. Clapp, A. H. MacDonald, and J. Zhu, Transport studies of dual-gated *ABC* and *ABA* trilayer graphene: Band gap opening and band structure tuning in very large perpendicular electric fields, Nano Lett. **13**, 369 (2013).

[44] T. Khodkov, I. Khrapach, M. F. Craciun, and S. Russo, Direct observation of a gate tunable band gap in electrical transport in *ABC*-trilayer graphene, Nano Lett. **15**, 4429 (2015).

[45] Y.-P. Wang, X.-G. Li, J. N. Fry, and H.-P. Cheng, First-principles studies of electric field effects on the electronic

structure of trilayer graphene, Phys. Rev. B **94**, 165428 (2016).

[46] L.-J. Yin, H. Jiang, J.-B. Qiao, and L. He, Direct imaging of topological edge states at a bilayer graphene domain wall, Nat. Commun. **7**, 11760 (2016).

[47] G. M. Rutter, S. Jung, N. N. Klimov, D. B. Newell, N. B. Zhitenev, and J. A. Stroscio, Microscopic polarization in bilayer graphene, Nat. Phys. **7**, 649 (2011).

[48] W. Yan, S.-Y. Li, L.-J. Yin, J.-B. Qiao, J.-C. Nie, and L. He, Spatially resolving unconventional interface Landau quantization in a graphene monolayer-bilayer planar junction, Phys. Rev. B **93**, 195408 (2016).

[49] S.-Y. Li, H. Liu, J.-B. Qiao, H. Jiang, and L. He, Magnetic-field-controlled negative differential conductance in scanning tunneling spectroscopy of graphene *npn* junction resonators, Phys. Rev. B **97**, 115442 (2018).

[50] B. Šopík, J. Kailasvuori, and M. Trushin, Charge transport in two dimensions limited by strong short-range scatterers: Going beyond parabolic dispersion and Born approximation, Phys. Rev. B **89**, 165308 (2014).